Real Mission Profile Based Lifetime Estimation of Fuel-cell Power Converter

Zhou, Dao; Wang, Huai; Blaabjerg, Frede; Kær, Søren Knudsen; Hansen, Daniel Blom

Published in:
Proceedings of 2016 IEEE 8th International Power Electronics and Motion Control Conference (IPEMC-ECCE Asia)

DOI (link to publication from Publisher):
10.1109/IPEMC.2016.7512741

Publication date:
2016

Real Mission Profile Based Lifetime Estimation of Fuel-cell Power Converter

Dao Zhou[1], Huai Wang[1], Frede Blaabjerg[1], Soeren Knudsen Kaer[1], Daniel Blom-Hansen[2]

[1] Department of Energy Technology
Aalborg University, Aalborg, Denmark
{zda, hwa, fbl, skk}@et.aau.dk

[2] Dantherm Power A/S
Hobro, Denmark
dbh@dantherm.com

***Abstract* - Fuel cells are becoming a promising energy source for various applications due to its relatively high efficiency and reliability, and low pollution. They have been applied in backup power systems in telecom applications, where reliability and availability are high priority performance factors. This paper describes a lifetime prediction method for the power semiconductors used in the power conditioning of a fuel cell based backup system, considering both the long-term standby mode and active operation mode. The annual ambient temperature profile is taken into account to estimate its impact on the degradation of MOSFETs during the standby mode. At the presence of power outages, the backup system is activated into the operation mode and the MOSFETs withstand additional thermal stresses due to power losses. A study case of a 1 kW backup system is presented with two annual mission profiles in Denmark and India, respectively. The ambient temperature, occurrence frequency of power outages, active operation time and power levels are considered for the lifetime prediction of the applied MOSFETs. Comparisons of the accumulated lifetime consumptions are performed between standby mode and operation mode, and between Denmark and India, respectively.**

I. INTRODUCTION

Fuel cells are widely recognized as one of the most promising convention technologies due to the relatively efficiency (i.e. approaching 60% and almost twice of that of the conventional combustion energies) [1]. Meanwhile, the scalability of fuel cells allows extensive applications from low power to high power [2]. For example, the fuel cells are an emerging candidate for backup power telecom application, because of its high energy density, high reliability, and less pollution [1], [3], [4]. As a telecom system is possibly connected to a remote electrical grid, the frequent interruptions put high priority on the availability and the reliability of the backup power system. Field experience has shown that the power conditioning stage is one of the system components responsible for most system failures, and it can be regarded as a critical assembly. Since the power semiconductor is a fragile element in the power electronic converters, this paper focuses on its lifetime estimation on the basis of the thermally-induced degradation.

Many research efforts have been devoted to the reliability prediction of power converters used in wind and photovoltaic power generation, which are normally the IGBT based dc/ac converters [5]-[8]. This paper extends to investigate the reliability metrics of dc/dc converters in the fuel cell system, where MOSFETs are the primary choice. Moreover, the mission profiles in backup power applications are unique, featuring with long time of the standby mode operation, as well as the active operation mode at the presence of power outages.

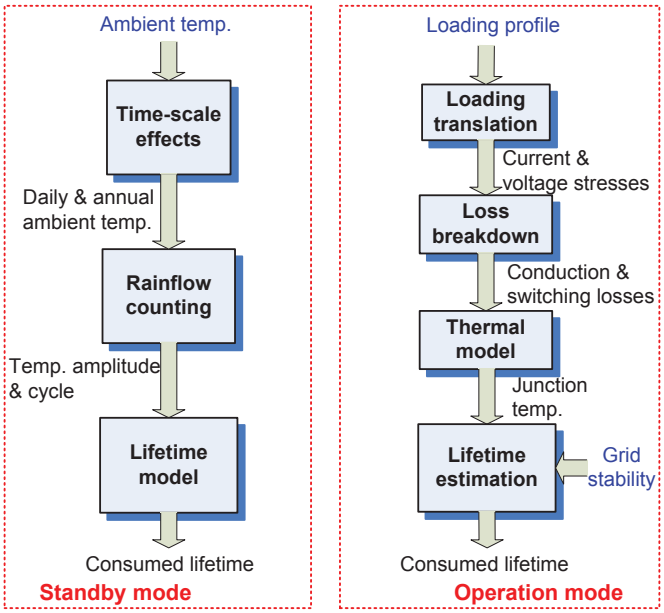

Fig. 1. A framework to predict lifetime of power switches used in a fuel cell backup power system in terms of standby mode and operation mode.

The structure of this paper is organized as follows in accordance with the framework shown in Fig. 1. Section II describes the mission profile of the fuel cell system used in telecom backup power. Section III discusses the thermal stress of the power switches by means of the yearly and the daily ambient temperature profiles during the standby mode. Section IV addresses the approach to analyze the thermal

978-1-5090-1210-7/16/$31.00 ©2016 IEEE

mapping of the power switches during the operation mode. Section V estimates the lifetime of the power switches by considering the two operation modes, followed by the conclusions.

II. Mission Profile Description of a Fuel Cell System

The Proton-Exchange-Membrane (PEM) fuel cell is normally selected as an alternative backup power used in telecom applications, due to its low operation temperature, relatively fast response time, and light-weight compared to traditional batteries and diesel generators. As shown in Fig. 2, the Balance of Plant (BoP) regulates the pressure of fuel and air before they enter into a fuel cell stack, and keeps the fuel cell at a reasonable temperature by controlling the coolant loop. The fuel cell stack converts the chemical energy to electricity through an electrochemical reaction. Afterwards, a power conditioner is applied to provide a stable dc-bus used in telecom application from the varying stack output voltage.

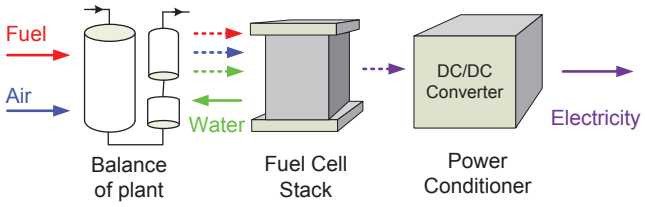

Fig. 2. Typical configuration of a fuel cell system.

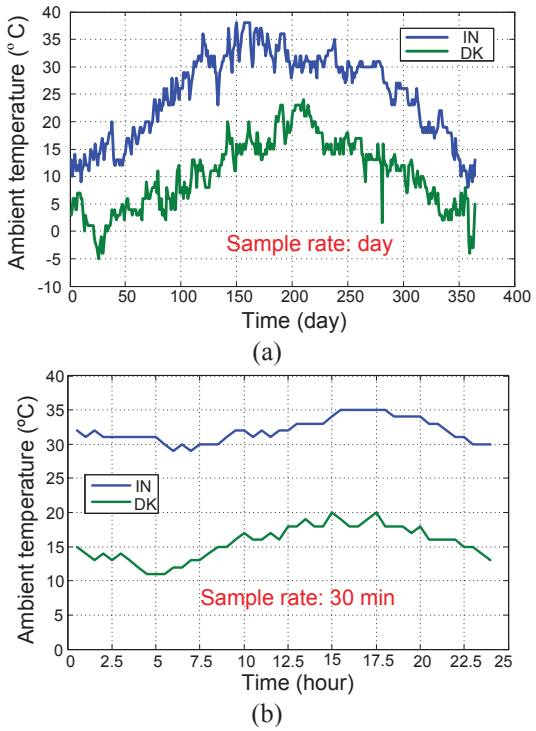

Fig. 3. Ambient temperature profile of Denmark (DK) and India (IN). (a) Yearly temperature of 2014; (b) Daily temperature of Jul. 1st, 2014.

Considering two applications in Denmark and India, the ambient temperature profiles are shown in Fig. 3 on the basis of history data of the global weather report [9]. The yearly ambient temperature profiles are sampled with the average daily temperature, while the daily temperature profiles are with a sample rate of 30 minutes.

For the backup power application, its working stage mainly consists of the standby mode and operation mode, depending on the grid condition of the local network. The typical grid conditions of Denmark and India are summarized in Table I in terms of the outage frequency and the outage duration. It can be observed that the backup power system operates much more frequent in India.

Table I

Annual Description of Typical Danish and Indian Grid Conditions

	Denmark	India
Outage frequency	2	365
Outage duration	10 min	4 hour

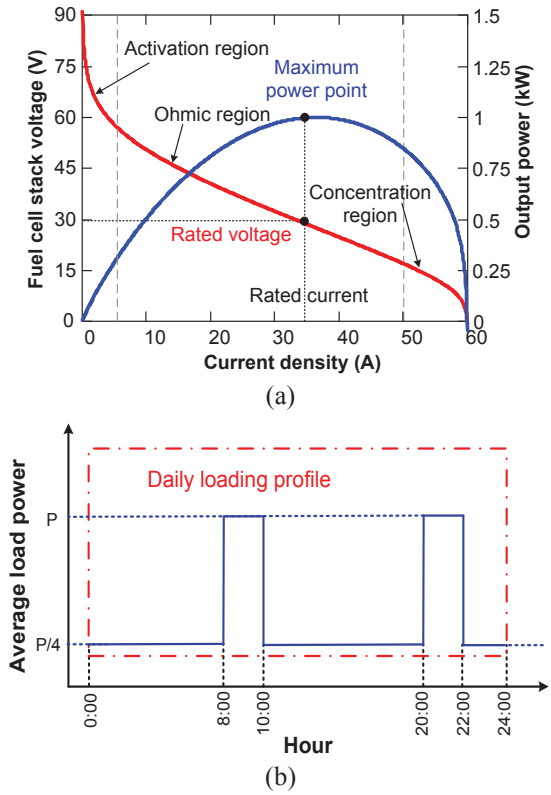

Fig. 4. The input power and output load of the power conditioner. (a) Output voltage and power of a fuel cell in relationship with current density; (b) A selected daily loading profile for the telecom application fed by either main power supplies or backup systems at the presence of power outages [4].

Loading condition is always an important constitution of the mission profile. In respect to the operation points of the

dc/dc power converter, both its input and output characteristics are required and shown in Fig. 4. As the input characteristic of power converter, the relationship between the output voltage and current density of the fuel cell stack is derived in Fig. 4(a) In general, the output voltage curve consists of three distinct regions – the activation, ohmic and concentration region [10]. The maximum power point appears in the ohmic region, and the power converter normally operates within the ohmic region. Meanwhile, a selected daily loading profile of the telecom application is addressed in [4], with 2 hours of full load and 10 hours of quarter load, and it is repeated every 12 hours as shown in Fig. 4(b). It is worth mentioning that different with the ambient temperature and the grid condition, the loading profile is the same regardless of locations in Denmark or India.

III. Thermal Stress Analysis of Standby Mode

In the case of the standby mode, the dc/dc converter is in off-state, and the junction temperature of the MOSFETs can roughly be considered the same with the ambient temperature. Assuming the similar and repeated annual climate in a certain location, its ambient temperature profile during the whole year can be used to analyze its thermal stress and then the annual accumulated damage. As shown in Fig. 3(a), the yearly ambient temperature in Denmark and India is depicted. It can be seen that the temperature fluctuates in both cases among different days. In order to evaluate the temperature fluctuation within one day, the daily ambient temperature profile is described in Fig. 3(b). It can be observed that the temperature becomes smoother with the sample rate of 30 min, due to the relatively higher inertia of the environment. For the simplification of the data processing, the daily temperature fluctuation in different days is assumed identical.

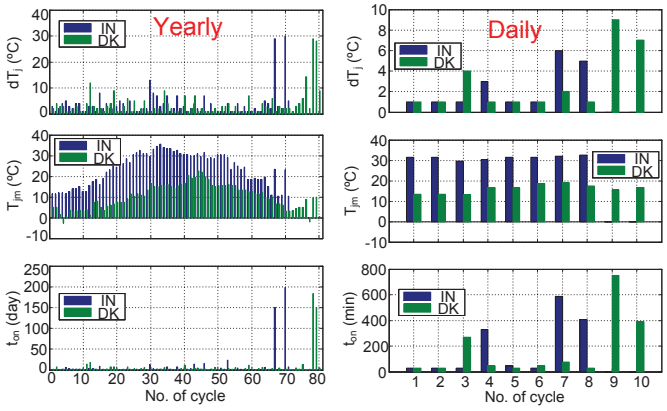

Fig. 5. Rainflow counting of the Danish and Indian ambient temperatures. (a) Yearly temperature profile; (b) Daily temperature profile.

Regardless of the yearly and daily ambient temperature profile, both of them perform in an irregular and complex manner. In order to reduce a spectrum of varying stress into a set of simple stress reversals, the Rainflow counting algorithm can be introduced, and amplitude, mean value as well as the period of each cycling can be exacted [11]. In respect to the Rainflow counting of the yearly profile as shown in Fig. 5(a), the maximum junction temperature swing dT_j in Denmark and India is almost the same because of the similar temperature difference between their maximum and minimum values. Moreover, India has a higher mean junction temperature T_{jm} compared to Denmark due to its overall higher ambient temperature. With the half period of each cycle t_{on}, it can be seen that the total counted cycles may be different in these two cases. The Rainflow counting can be extended to analyze the daily temperature in Fig. 3(b), and a lower temperature swing but a higher mean temperature of India is observed in Fig. 5(b). Generally speaking, the yearly temperature contributes on the investigation of the seasonal climate effects, and daily temperature evaluates the temperature cycling caused by alternating day and night.

IV. Thermal Stress Analysis of Operation Mode

In order to assess the lifetime of MOSFET, this section starts with the investigation and evaluation in respect to the loss mapping and thermal profile of the power semiconductor. It is worth mentioning that only MOSFETs used in converter primary-side are focused in this study.

A. Voltage and current stresses of MOSFETs

Among numerous power converters of the fuel cell application, the isolated full-bridge boost converter is the most popular. As shown in Fig. 6, the isolated dc/dc power converter is adopted due to its reduced component stresses compared to an isolated full-bridge [11], [12]. In the primary-side, it consists of an input inductor L, and three bridge legs (Q_1-Q_2, Q_3-Q_4, Q_5-Q_6), which are used to drive two individual transformers (T_1, T_2). In the secondary-side, two full bridge rectifiers (D_1-D_4, D_5-D_8) are connected in parallel to the output. To cope with the wide range of the input voltage, this converter is able to operate in both the step-up mode and the step-down mode depending on whether the input voltage is lower or higher than the reflected output voltage of the transformer primary-side. The key waveforms of the dc/dc power converter are shown in Fig. 7.

When the power converter operates in the step-up mode, the inductor is charged with the activation of the all transistors, while it is discharged with the parallel connection of the transformers as shown in Fig. 7(a). The center leg switches carry full inductor current whereas the side legs only carry half of the inductor current during the discharge period. In order to have a matched current stress among different switches, two paralleled transistor are used in the center leg. Due to the identical waveform of the paralleled transistors, the current and voltage waveform of the transistors can simply be described from Q_1 to Q_5.

In the case of the step-down mode, the inductor is charged with the parallel connection of transformers, and it is discharged with the series connection of transformers. According to output characteristics of the fuel cell stack, its voltage becomes higher and the current becomes lower in the light load condition. As a consequence, the converter may

operate in either the Continuous Current Mode (CCM) or the Discontinuous Current Mode (DCM). If the CCM is taken into account, it is obvious that the current stresses of side legs and the center leg are different as shown in Fig. 7(b). Side legs carry maximum full inductor current, while the center leg only conducts half of the inductor current. Nevertheless, the high-side and the low-side switches in the same leg withstand the identical voltage and current stresses. If the load becomes light enough, the converter operates in the DCM. Compared to the CCM, as the inductor current decreases to zero during the periods when Q_1 and Q_6, or Q_2 and Q_5 are in on-state, there are two additional stages when the load is entirely supplied by the output storage capacitor.

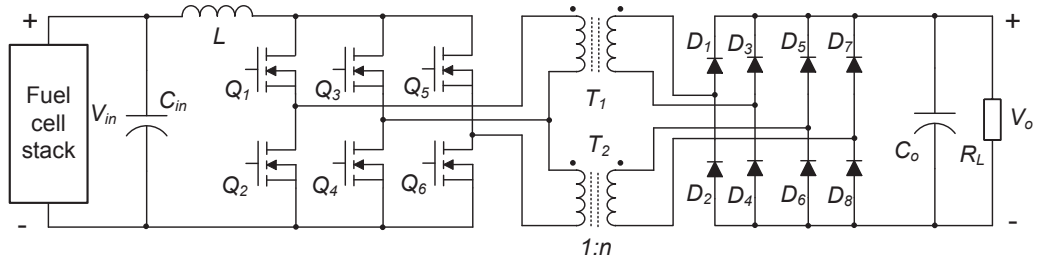

Fig. 6. 1 kW dc/dc power converter used in the fuel cell system.

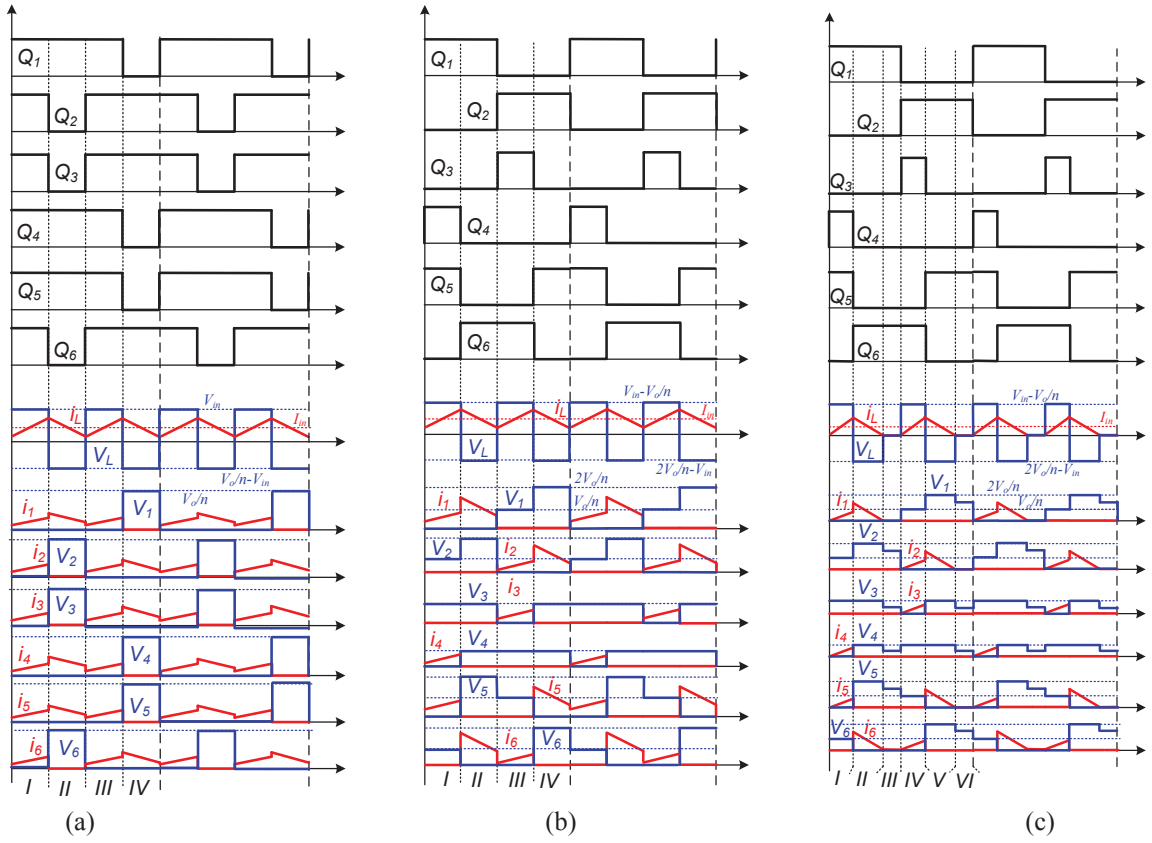

Fig. 7. Key waveforms of the dc/dc power converter. (a) Step-up mode; (b) Step-down mode with continuous current mode; (c) Step-down mode with discontinuous current mode.

A 1 kW power converter is used as a case study, and its specifications and main design parameters are listed in Table II. Eight MOSFETs are selected in the primary-side, and the switching frequency is 50 kHz. Meanwhile, some typical operation points of the power converter can be found in Table III. It can be seen that input voltage decreases with increasing load. The power converter switches from the step-down mode to the step-up mode when the output power reaches around

half of the rated value. Moreover, if the load is less than 125 W, the converter operates in DCM.

Table II

CONVERTER SPECIFICATIONS AND PARAMETERS

Input voltage V_{in}	30 – 65 V
Output voltage V_o	48 V
Maximum output power P_o	1000 W
Primary-side MOSFET	100 V/74 A, ×8
Input inductor L	15 μH
Transformer turns ratio n	1:1
Switching frequency f_{sw}	50 kHz

Table III

TYPICAL OPERATION POINTS OF POWER CONVERTER

Output power (W)	Input voltage (V)	Operation mode	Inductor current	Duty cycle
125	65	Step-down	DCM	23.4%
250	60	Step-down	CCM	37.5%
375	55	Step-down	CCM	42.7%
500	50	Step-down	CCM	47.9%
625	45	Step-up	CCM	53.1%
750	40	Step-up	CCM	58.3%
875	35	Step-up	CCM	63.5%
1000	30	Step-up	CCM	68.8%

B. Power loss analysis

The power losses of MOSFETs mainly consist of the conduction loss and the switching loss [13]. For the conduction loss, as the voltage drop across the MOSFET can be deduced by the product of the drain current i_D and the drain-source on-state resistance R_{DSon}, the conduction loss P_{con} is that the accumulation of the voltage drop and drain current within one switching period T_{sw} multiplies the switching frequency f_{sw}, which can be calculated as,

$$P_{con} = f_{sw} \cdot \int_0^{T_{sw}} R_{DSon} \cdot i_D{}^2(t)dt \quad (1)$$

where the maximum value of the drain-source on-state resistance is selected for the worse scenario, which is given in the manufacturer datasheet.

Due to the existence of the current commutation and Miller plateau during the switch-on transient and the switch-off transient of the MOSFET, the drain-source voltage and the drain current cannot be changed abruptly. The overlapping of transient voltage and current contributes on the switching loss P_{sw}, and it can be calculated as

$$P_{sw} = f_{sw} \cdot \left(\frac{V_{DS\_on} \cdot I_{D\_on} \cdot (t_{ri} + t_{fu})}{2} + \frac{V_{DS\_off} \cdot I_{D\_off} \cdot (t_{ru} + t_{fi})}{2}\right) \quad (2)$$

where the first term stands for the turn-on loss P_{on} and the second term stands for the turn-off loss P_{off}. V_{DS_on} denotes the blocking drain-source voltage before the MOSFET is switched on, I_{D_on} denotes the initial turn-on drain current, t_{ri} denotes turn-on rise time of the conducting current indicated in the manufacturer datasheet, and t_{fu} denotes the fall time of the blocking voltage deduced by using two-point approximation as mention in [13]. In contrast, V_{DS_off} denotes the initial blocking drain-source voltage when the MOSFET is switched off, I_{D_off} denotes the final turn-on drain current, t_{ru} denotes the turn-off rise time of the blocking voltage calculated by using similar approach as t_{fu}, and t_{fi} denotes the turn-off fall time provided by the manufacturer datasheet.

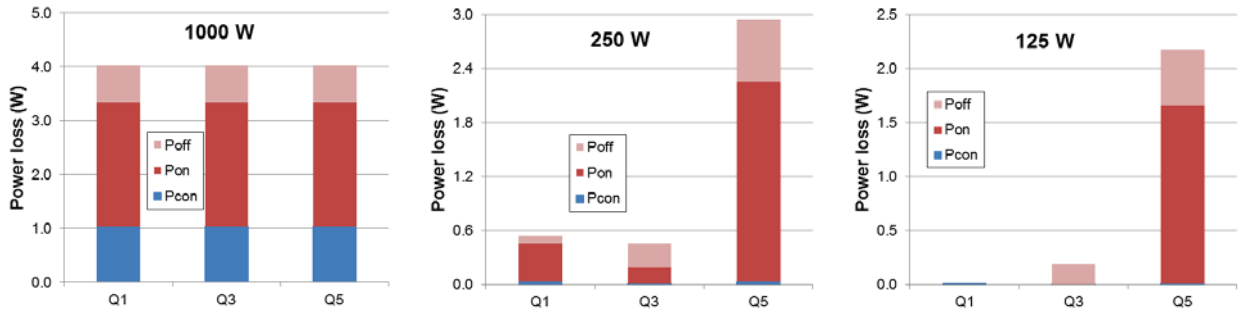

Fig. 8. Power loss distribution of MOSFETs. (a) Step-up mode at 1000 W; (b) Step-down mode with continuous current mode at 250 W; (c) Step-down mode with discontinuous current mode at 125 W.

As summarized in Table III, the power converter may operate in step-up CCM, step-down CCM, and step-down DCM depending on the load conditions. Consequently, the loading conditions at 1000 W, 250 W, and 125 W are chosen and their loss distribution is calculated according to (1) and (2). Due to the same loading of high-side and low-side MOSFETs, the loss distribution of Q_1, Q_3 and Q_5 are shown in Fig. 8. In the case of the step-up mode at the loading of 1000 W, Q_1, Q_3 and Q_5 are equally stressed because of the same loading current and blocking voltage. If the converter works in step-down mode with CCM at the loading of 250 W, it is noted that the conduction losses of the side leg switches are the same, which are higher than that of the center leg switches due to their longer conduction period. However, the switching

losses of three legs become unbalanced because of different blocking voltages and drain currents during switching transitions. As a consequence, the loss dissipation among the switches of three bridge legs becomes significantly unequal, in which Q_5 is the most stressed. In the step-down mode with DCM at loading of 125 W, the conduction losses in the side legs are still higher than the center leg. In regard to the switching loss, Q_1 has no switching loss due to the zero current during the turn-on and the turn-off transitions. Similarly, it can be noted that Q_3 has turn-off switching loss only. However, both the turn-on and the turn-off loss appear in Q_5 because the commutated current remains during the transient period. In addition, the switching losses are dominating in all three cases compared with the conduction losses.

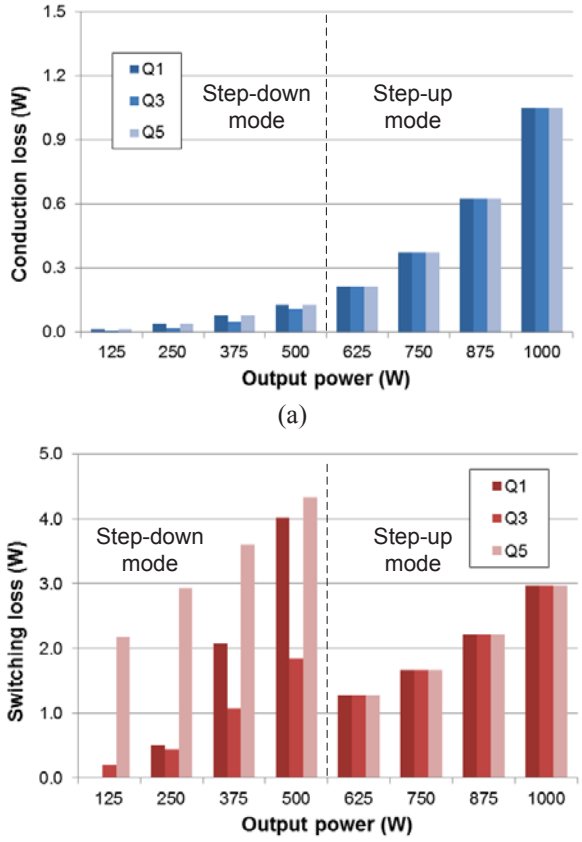

Fig. 9. Loss mapping of MOSFETs with increasing output power. (a) Conduction loss; (b) Switching loss.

The loss mapping of the MOSFETs with the increasing output power is shown in Fig. 9, in which the conduction loss and the switching loss are described, respectively. It can be seen that both the conduction loss and the switching loss become significantly unequal in the case of the step-down mode, while they are balanced if the converter operates in the step-up mode. For the conduction loss, it increases with the higher output power, as the input current and duty cycle become higher. Regardless of the step-down mode or the step-up mode, if the converter remains working in the same mode, the switching loss keeps increasing. However, if the converter changes from the step-down mode to the step-up mode, the switching loss decreases. It is because in spite of higher output voltage, the blocking voltage of the MOSFET becomes higher. Additionally, it is evident that Q_5 is the most stressed regardless of the operation modes.

C. Thermal profile

As the junction temperature of MOSFETs affects many operation parameters and device lifetime, the thermal stress of the power devices is then investigated and evaluated. Neglecting the thermal couple from adjacent devices, each MOSFET can be regarded as an independent thermal system due to its package.

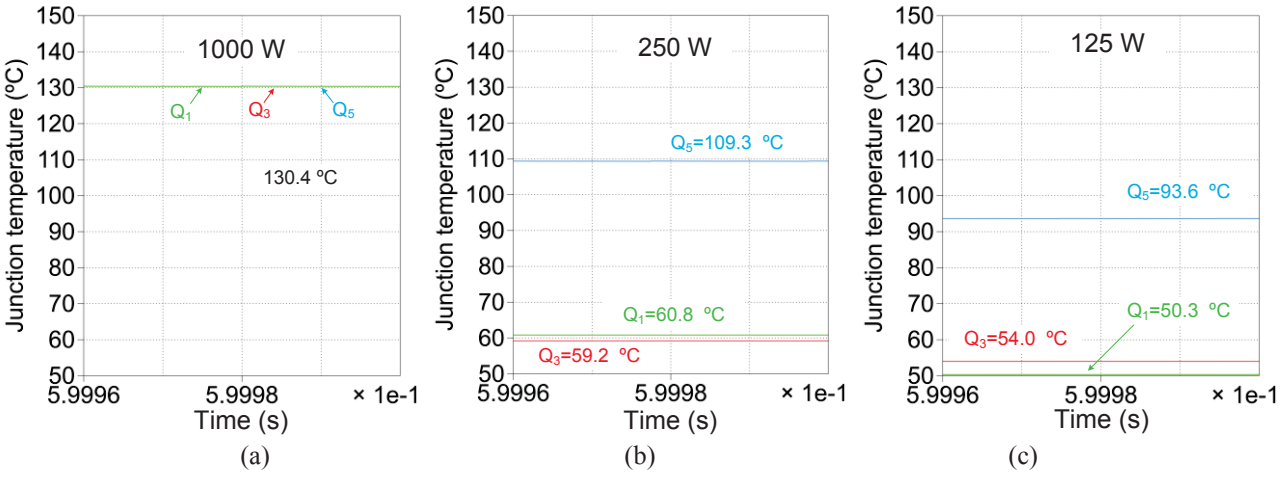

Fig. 10. Junction temperature of MOSFETs at typical operation modes. (a) Step-up mode at 1000 W; (b) Step-down mode with continuous current mode at 250 W; (c) Step-down mode with discontinuous current mode at 125 W.

According to a single pulse thermal response curve provided by the manufacturer, the thermal impedance from the junction to case can be obtained by using a four-layer Foster model [14]. Besides, as the thermal time constant of the heatsink is much higher than the MOSFET itself, only the thermal resistance is taken into account, which can also be acquired from the datasheet. Assuming that the ambient temperature is 50 ºC, the junction temperature can be simulated by using PLECS. As shown in Fig. 10, the junction temperature of three typical operation modes in step-up CCM, step-down CCM, and step-down DCM are analyzed. Similar to the loss distribution, Q_1, Q_3 and Q_5 share the same junction temperature in the step-up mode, while they become significantly unbalanced if operating in the step-down mode. It is noted that all the junction temperatures keep constant at the steady-state at a given load level with negligible temperature swing, because the temperature variation within one switching cycle is insignificant due to the thermal inertias.

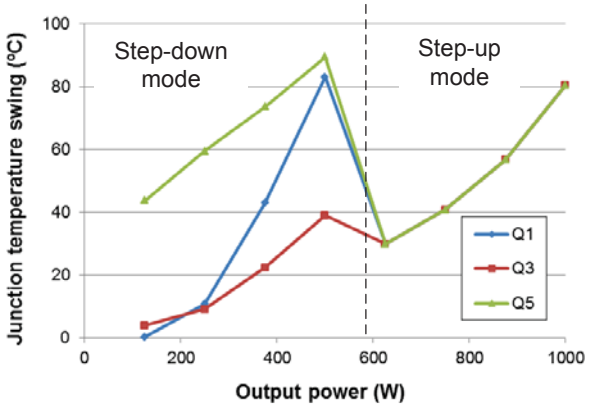

Fig. 11. Junction temperature swing of MOSFET with various output power.

The junction temperature swing for each MOSFET can be summarized in Fig. 11 at various loading conditions. In the case of the step-down mode, the junction temperature of Q_3 and Q_5 increases with load in a moderate manner, while Q_1 increases much more rapidly. In the case of the step-up mode, junction temperature of three legs becomes the same, and it continuously increase with higher output power. It can be seen that MOSFET Q_5 is always most stressed, and it reaches its highest junction temperature at the end of the step-down mode. Although the reliability of the converter products is affected by every power switches, the power switch Q_5 has the shortest lifetime compared to other switches, and the following lifetime estimation is mainly focused on this component.

V. Lifetime Estimation Based on Mission Profile

As previously mentioned, in the case of the standby mode, the junction temperature of the MOSFET can roughly be considered the same with the ambient temperature. During the operation period, the junction temperature of the MOSFET is determined by the loading condition of the fuel cell system, which is related to the aforementioned thermal profile. The approach to estimate the lifetime contribution of each working mode is explained and addressed, where two typical mission profiles from Denmark and India are compared.

A. Standby mode

By using Coffin-Manson model [15], [16], the power cycles before the failure occurrence N_f can be expressed as,

$$N_f = A \cdot dT_j^{\beta_1} \cdot \exp\left(\frac{\beta_2}{T_{jm}+273}\right) \cdot t_{on}^{\beta_3} \tag{3}$$

where the power cycles are closely related to the junction temperature swing dT_j, mean junction temperature T_{jm} as well as the its on-time duration t_{on}. Besides, A, β_1, β_2, and β_3 can be obtained according to test data provided by the manufacturer.

According to Miner's rule - linear damage hypothesis [17], the failure occurs when the sum of stress cycles at different magnitudes n over their corresponding number of cycles to failure N_f reaches 1. As a consequence, the annual consumed lifetime or the annual damage CL can be defined as,

$$CL = \sum \frac{n_{(i)}}{N_{f(i)}} \tag{4}$$

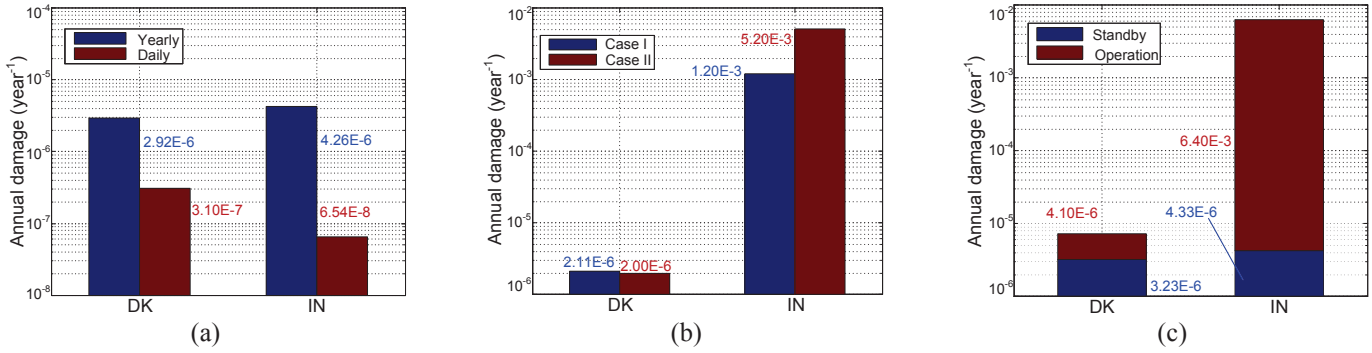

Fig. 12. Annual damage comparison of MOSFET between Danish and Indian mission profiles. (a) Effects of standby mode; (b) Effects of operation mode; (c) Total effects of operation mode and standby mode.

On the basis of Rainflow counting as shown in Fig. 5, the annual damage comparison between Danish and Indian mission profiles is shown in Fig. 12(a). The yearly temperature consumes higher lifetime due to its considerably higher temperature fluctuation and much longer period of thermal cycling compared with the daily temperature effects.

B. Operation mode

In the case of the grid outage, the fuel cell system operates as a backup power, and the thermal profile of the MOSFET is determined by loading conditions. As the grid outage happens randomly, two kinds of the loading profile (quarter load *Case I* or full load *Case II*) may be imposed to the power converter with various probabilities of each event. Assuming that the ambient temperature is set at 25 ºC and 40 ºC for the worst scenario, the mean junction temperature and the junction temperature swing can be calculated according to Fig. 11. In addition, the on-time duration is same with the grid outage duration, and number of thermal cycling is determined by the outage frequency.

As a result, the effects of the operation modes on the consumed lifetime are shown in Fig. 12(b). For the Danish mission profile, *Case II* has the similar consumed lifetime compared with *Case I*. For the Indian mission profile, although *Case I* occurs the most frequently, *Case II* has the highest consumed lifetime due to its severest thermal cycling.

C. Total lifetime estimation

As shown in Fig. 12(c), the total annual damage is the sum the standby mode and the operation mode. In Danish case, both the standby mode and the operation mode almost contribute the same on the lifetime consumption due to less frequency but higher thermal stress of the operation mode. In India case, even though the fuel cell system mostly works in the standby mode, the operation mode dominates the lifetime consumption. In addition, the Indian mission profile has the total consumed lifetime of 6.40E-3 compared to the Danish mission profile of 7.33E-6, which indicates that the expected lifetime of MOSFET Q_5 in Denmark is almost 873 times higher.

VI. CONCLUSION

This paper proposed an approach to predict the lifetime of power semiconductors in a fuel cell based backup power system. The annual mission profile under both standby mode and operation mode is taken into account. A 1 kW dc/dc converter study case reveals: 1) thermal stresses of various MOSFETs in the analyzed dc/dc converter are different in the step-down mode; 2) the annual lifetime consumption is dominated by the operation mode even though the total operation time is much shorter than that of standby mode; 3) the estimated lifetime of the most stressed MOSFET under a severe mission profile in India is significantly shorter than that in Denmark with much less power outages. Therefore, it is of importance to design the dc/dc converter by considering the thermal loading management of power semiconductors, and the impact of the diversity in mission profiles.

ACKNOWLEDGEMENT

The authors acknowledge the financial support from Danish Energy Technology Development and Demonstration Program through the REST (Reliability ESTimation of hydrogen and fuel cell systems) project.

References

[1] K. Rajashekara, "Hybrid fuel-cell strategies for clean power generation," *IEEE Trans. on Industry Applications*, vol. 41, no. 3, pp. 682-689, May 2005.

[2] X. Yu, M. R. Starke, L. M. Tolbert, and B. Ozpineci, "Fuel cell power conditioning for electric power applications: a summary," *IET Electric Power Applications*, vol. 1, no. 5, pp. 643-656, Sep. 2007.

[3] H. Tao, J. L. Duarte, and M. A. M. Hendrix, "Line-interactive UPS using a fuel cell as the primary source," *IEEE Trans. on Industrial Electronics*, vol. 55, no. 8, pp. 3012-3021, Aug. 2008.

[4] M. J. Vasallo, J. M. Andujar, C. Garcia, and J. J. Brey, "A methodology for sizing backup fuel-cell/battery hybrid power systems," *IEEE Trans. on Industrial Electronics*, vol. 57, no. 6, pp. 1964-1975, June 2010.

[5] H. S. Chung, H. Wang, F. Blaabjerg, and M. Pecht, *Reliability of power electronic converter systems*. Institution of Engineering and Technology, 2015.

[6] K. Ma, M. Liserre, F. Blaabjerg, and T. Kerekes, "Thermal loading and lifetime estimation for power device considering mission profiles in wind power converter," *IEEE Trans. on Power Electronics*, vol. 30, no. 2, pp. 590-602, Feb. 2015.

[7] Y. Yang, H. Wang, F. Blaabjerg, and K. Ma, "Mission profile based multi-disciplinary analysis of power modules in single-phase transformerless photovoltaic inverters," *in Proc. of EPE 2013*, pp.1-10, 2013.

[8] D. Zhou, F. Blaabjerg, M. Lau, and M. Tonnes, "Optimized reactive power flow of DFIG power converters for better reliability performance considering grid codes," *IEEE Trans. on Industrial Electronics*, vol. 62, no. 3, pp. 1552-1562, Mar. 2015.

[9] Global weather report. (http://www.wunderground.com/)

[10] G. Zhu, K. H. Loo, Y. M. Lai, and C. K. Tse, "Quasi-maximum efficiency point tracking for direct methanol fuel cell in DMFC/supercapacitor hybrid energy system," *IEEE Trans. on Energy Conversion*, vol. 27, no. 3, pp. 561-571, Sep. 2012.

[11] M. Matsuishi, and T. Endo, "Fatigue of metals subjected to varying stress", *Japan Soc. Mech. Engineering*, 1968.

[12] L. P. Petersen, L. C. Jensen, and M. N. Larsen, "High efficiency isolated DC/DC converter inherently optimized for fuel cell applications," *in Proc. of EPE 2013*, pp.1-10, 2013.

[13] Infineon, *MOSFET power losses calculation using the datasheet parameters*.

[14] Alpha & Omega semiconductor, *Thermal resistance characterization of Power MOSFETs*.

[15] A. Wintrich, U. Nicolai, and T. Reimann, *Semikron Application Manual*, p. 128, 2011.

[16] U. Scheuermann, and R. Schmidt, "A new lifetime model for advanced power modules with sintered chips and optimized Al wire bonds," *in Proc. of PCIM 2013*, pp. 810–813, 2013.

[17] H. C. Yildirim, G. Marquis, and Z. Barsoum, " Fatigue assessment of high frequency mechanical impact (HFMI)-improved fillet welds by local approaches," *International Journal of Fatigue*, vol. 52, pp. 57–67, 2013.